Review of Scientific Instruments

Internal resistive heating of non-metallic samples to 3000 K and >60 GPa in the diamond anvil cell

Cite as: Rev. Sci. Instrum. **92**, 063904 (2021); https://doi.org/10.1063/5.0038917
Submitted: 27 November 2020 . Accepted: 15 May 2021 . Published Online: 11 June 2021

Benedict J. Heinen, James W. E. Drewitt, Michael J. Walter, Charles Clapham, Fei Qin, Annette K. Kleppe, and Oliver T. Lord

AIP Publishing

Review of Scientific Instruments ARTICLE scitation.org/journal/rsi

Internal resistive heating of non-metallic samples to 3000 K and >60 GPa in the diamond anvil cell

Cite as: Rev. Sci. Instrum. 92, 063904 (2021); doi: 10.1063/5.0038917
Submitted: 27 November 2020 • Accepted: 15 May 2021 •
Published Online: 11 June 2021

Benedict J. Heinen,[1,a] James W. E. Drewitt,[1,2] Michael J. Walter,[3] Charles Clapham,[1] Fei Qin,[1] Annette K. Kleppe,[4] and Oliver T. Lord[1]

AFFILIATIONS

[1] School of Earth Sciences, University of Bristol, Wills Memorial Building, Queens Road, Bristol BS81RJ, United Kingdom
[2] School of Physics, University of Bristol, HH Wills Physics Laboratory, Tyndall Avenue, Bristol BS81TL, United Kingdom
[3] Earth and Planets Laboratory, Carnegie Institution for Science, 5241 Broad Branch Road NW, Washington, DC 20015, USA
[4] Diamond Light Source Ltd., Diamond House, Harwell Science and Innovation Campus, Didcot, Oxfordshire OX110DE, United Kingdom

[a] **Author to whom correspondence should be addressed:** benedict.heinen@bristol.ac.uk

ABSTRACT

High pressure–temperature experiments provide information on the phase diagrams and physical characteristics of matter at extreme conditions and offer a synthesis pathway for novel materials with useful properties. Experiments recreating the conditions of planetary interiors provide important constraints on the physical properties of constituent phases and are key to developing models of planetary processes and interpreting geophysical observations. The laser-heated diamond anvil cell (DAC) is currently the only technique capable of routinely accessing the Earth's lower-mantle geotherm for experiments on non-metallic samples, but large temperature uncertainties and poor temperature stability limit the accuracy of measured data and prohibits analyses requiring long acquisition times. We have developed a novel internal resistive heating (IRH) technique for the DAC and demonstrate stable heating of non-metallic samples up to 3000 K and 64 GPa, as confirmed by *in situ* synchrotron x-ray diffraction and simultaneous spectroradiometric temperature measurement. The temperature generated in our IRH-DAC can be precisely controlled and is extremely stable, with less than 20 K variation over several hours without any user intervention, resulting in temperature uncertainties an order of magnitude smaller than those in typical laser-heating experiments. Our IRH-DAC design, with its simple geometry, provides a new and highly accessible tool for investigating materials at extreme conditions. It is well suited for the rapid collection of high-resolution P–V–T data, precise demarcation of phase boundaries, and experiments requiring long acquisition times at high temperature. Our IRH technique is ideally placed to exploit the move toward coherent nano-focused x-ray beams at next-generation synchrotron sources.

I. INTRODUCTION

High pressure research is a rapidly advancing field. High pressure causes materials to undergo structural and electronic changes, affects the chemical reactivity of elements, and gives rise to a wide variety of exotic physical phenomena such as liquid–liquid (polyamorphic) transitions,[1–3] metallization,[4,5] and superionic[6] and superconducting[7] behavior. The phase diagrams of materials are important to fundamental condensed matter physics, and even the high-pressure behavior of elements and simple systems is an area of frontier research.[8,9] The application of pressure can stabilize exotic materials with unprecedented stoichiometries, chemical activity, bonding, or physical properties. Therefore, pressure (P) provides a powerful tuning parameter or synthesis pathway for a vast array of materials with desirable properties. These include superhard materials with a wealth of industrial uses,[10–12] novel superionic phases and high entropy oxides with important applications in next-generation battery technology,[13–15] high-energy-density materials for propellants,[16,17] novel polymorphs of pharmaceutical molecules,[18] electrides,[19] hydrogen storage materials,[20] and superconductors.[7] The addition of temperature (T) as another parameter expands the phase space for materials discovery or novel phenomena even further.[11,21–24] High temperature techniques can provide alternative synthesis pathways for materials similar to those

with recently reported room temperature superconducting properties.[7,22,23] The metallization of hydrogen at extreme pressures has been reported,[5,25] as has an analogous liquid metallic state of hydrogen stable at megabar pressures and temperatures over 1800 K that is thought to be the main constituent of gas giant planets.[21,26] Superionic states in hot dense molecular compounds such as solid H_2O, NH_3–H_2O, and NH_3–He mixtures have been created at high P–T conditions and are likely to be present in the interiors of icy giant planets.[6,24,27,28]

Recreating the extreme conditions of planetary interiors can provide the phase assemblage for a given bulk composition.[29–31] For the Earth, experimental constraints on the thermoelastic parameters of deep Earth materials are vital for the correct interpretation of observed seismic structure, but significant uncertainties currently exist for many of these parameters.[32] The lower mantle is of particular interest as it is the largest reservoir for many elements, stores a record of both planetary formation processes and the exchange of materials between the exosphere and deep interior over the course of Earth's history, and has seismic features that are still poorly understood.[33–38] Knowledge of the physical and chemical characteristics of the lower mantle therefore provides important constraints on the evolution of our planet.

There are many experimental techniques for generating high pressure and temperature conditions in the laboratory, but the extreme conditions required to study the lower mantle (~24–130 GPa, ~1900–3000 K) and to synthesize many of the novel materials described above present significant experimental difficulty. The primary apparatuses used for static pressure generation at these conditions are the Kawai-type multi anvil press (MAP) and the diamond anvil cell (DAC).

MAP apparatus are typically limited to ~20–30 GPa for routine experiments. Advances in experimental techniques, such as innovative anvil truncation designs and the use of sintered diamond anvils instead of the typical WC cubes, have pushed the MAP pressure limit well into the range of lower mantle conditions for some experimental setups, and pressures above 100 GPa have been reported, though are far from routine.[39–41] High temperatures are generated through the use of a resistive heater surrounding the sample assembly and are typically very stable, with precise measurements made via a thermocouple. However, temperature generation in MAP experiments above 30 GPa has typically been limited to <1500 K,[42–44] although a recent study reported stable heating at 2000 K and 50 GPa.[40] Nevertheless, much of the pressure–temperature (P–T) range of the lower mantle remains outside the capabilities of MAP techniques. Furthermore, the size of MAP apparatus makes them difficult to interface with *in situ* analysis techniques such as x-ray diffraction (XRD) and impractical to conduct multiple analyses using different techniques on the same sample.

In contrast, pressures encompassing the mantle can be generated routinely in the DAC. Unlike MAPs, the transparency of diamond anvils allows *in situ* optical analysis such as Raman, Fourier-transform infrared (FTIR), and Brillouin spectroscopy, and the portability of DACs means that they can be easily interfaced with a wide range of synchrotron x-ray techniques such as XRD, inelastic x-ray scattering (IXS), x-ray fluorescence (XRF), and x-ray absorption spectroscopy (XAS). Combined with laser heating, DACs can easily access the whole of the lower mantle geotherm. Typically, heating lasers operate at near-IR wavelengths (~1 μm) that are not absorbed by iron-free compositions, necessitating the mixing of the sample with a metallic absorber, which can lead to significant thermal gradients.[45] CO_2 lasers that operate at much longer wavelengths (~10 μm) can be directly absorbed by iron-free compositions and have a greater penetration depth into the sample (thereby lessening axial temperature gradients).[46] However, CO_2 lasers are more expensive, require specialist optics, are less stable, and are harder to align.[46,47] Compared to near-IR lasers, CO_2 lasers are also harder to interface with fiber-optics, which facilitate the design of more portable and flexible setups.[47] Temperatures are measured in laser-heated DAC experiments spectroradiometrically, which involves fitting a Wien function to the thermal emission collected from the heated region, often with an analytical precision of a few K on a single measurement.[48,49] However, the true uncertainty in the temperature of the analyzed sample volume over the timescale of the laser heating experiment is controlled by the size and intensity profile of the heating laser and, most importantly, the geometry and absorbance characteristics of the sample itself, which can vary significantly spatially and with time. Heterogeneous temperature during laser heating can cause diffusion of elements along thermal gradients.[45] Axial temperature gradients can be reduced by simultaneous laser-heating of both sides of the sample and by surrounding the sample with a thermal insulator, while improvements in laser heating optics, including the use of beam shaping to flatten the Gaussian intensity profile of the heating laser, can reduce radial temperature gradients.[49,50] Nevertheless, spatial and temporal fluctuations in temperature over the duration of an experiment lead to uncertainties that are typically 100 K or more.[38] Heating instability poses a particular problem for techniques requiring long data acquisition times, such as Brillouin spectroscopy and IXS,[51,52] and heating periods of less than an hour may be insufficient for the sample to reach thermodynamic equilibrium.[30]

Resistive heating techniques provide greater temperature stability, more precise control, reduced thermal gradients, and uncertainties that are an order of magnitude smaller.[53] External resistive heating, in which a heater surrounds the anvil assembly or entire DAC, is a commonly used technique. A wide range of designs exist, including commercially available options (e.g., Refs. 53–55). Designs often incorporate the use of thermocouples, which allows temperature measurement below the typical limit of spectroradiometry (~1200 K). Resistive heating techniques also enable melting of the entire sample, which is difficult to achieve with laser heating.[9,55] However, external heating techniques are typically limited to <~1300 K, beyond which the unpressurized parts of the diamond anvils begin to graphitize, and the other components of the cell deform. Several recently reported designs have pushed this limit to ~1500 K through the use of graphite heaters in combination with vacuum chambers and innovative cooling systems.[56,57] One successful run with a reported peak temperature of 1900 K also demonstrates the possibility for advancement of these techniques,[56] but significant experimental difficulty remains. Routine experiments replicating the conditions of the lower mantle are therefore not feasible with external resistive heating.

Internal resistive heating, in which heat is generated only within the pressure chamber and isolated from the diamonds, can extend the accessible temperature range drastically. Internal resistive heating techniques have previously been successful in the study of metals at high pressure and temperature, by electrically

heating a fine wire, compressed between the anvils, which serves as both the heating element and sample. This technique (often termed "fine-wire heating") was first pioneered by Liu and Bassett[58] and is now well established (e.g., Refs. 59–62). Recent experimental advances in this technique have proved useful in the study of melting[63] and resistivity[64] of metals; however, the application of internal resistive heating (IRH) to non-metallic samples has been limited.[65,66]

To achieve resistive heating inside a DAC pressure chamber, the electrical circuit must be carefully designed so that it runs through the heating filament and is not broken as the cell is compressed. This is typically done by running distinct electrodes into the pressure chamber, necessitating electrical isolation of the electrodes from other metallic components (i.e., the gasket) to prevent a short. Existing designs rely on a composite gasket to do this, employing a layered,[60,61,67,68] concentric,[62–64,69] or combined design.[65,70] The use of a composite gasket introduces significant manufacturing complexity and can lead to pressure limitations due to reduced structural integrity.[65] Furthermore, in these designs, the heater cannot be completely isolated from the diamonds, and the filament or electrodes must directly contact diamond along the electrical pathway into the pressure chamber. This can create a temperature limit as heating outside of the insulated sample chamber can lead to failure of the anvils due to thermal weakening and/or graphitization or draw heat away from the sample due to the unusually high thermal conductivity of diamond.[66] One solution is to design the heater such that the insulated portion of the filament has a much greater electrical resistance relative to the external leads. This is commonly achieved by reducing the cross-sectional area of the filament. Several designs using this approach are capable of generating temperatures of several thousand K at multi-megabar pressures but employ filaments too small to accommodate a separate sample.[63,64]

An alternative approach is to use a material with a much greater intrinsic resistivity. Ozawa *et al.*[70] recently suggested boron-doped diamond (BDD) as a promising candidate material, as its resistivity is around five orders of magnitude greater than the Pt or W electrical leads used in their design (depending on Boron content). While this strategy achieved maximum heater temperatures of 3580 K at 28 GPa and 2580 K at 43 GPa, it has not yet been adapted to contain a distinct sample chamber and relies on surrounding the heater with a silicate sample material that also acts as the pressure medium, leading to maximum sample temperatures much lower than those of the hottest part of the heater and introducing large temperature gradients. The use of BDD also introduces significant fabrication complexity, necessitating a MAP apparatus to synthesize the heater material and the use of an argon ion beam to prepare the filament.[70]

Zha and Bassett[65] and Zha *et al.*[66] previously reported x-ray diffraction and Raman scattering measurements of non-metallic materials measured in an internally resistive heated DAC. The design of Zha and Bassett[65] employed a combined composite gasket approach, with an outer layered composite gasket and an inner (concentric) solid gasket. The outer gasket consisted of an insulation layer sandwiched between two stainless steel supporting gaskets to which the electrical leads were welded, and the inner gasket was composed of a fine grained (1 μm) mixture of diamond (30 vol. %) and MgO (70 vol. %) powders compressed in the outer gasket (with the entire culet region drilled out) for more than 1 h at >5 GPa. The pressure chamber was drilled into the inner gasket and a rhenium heating filament threaded through the chamber to connect the upper and lower outer gaskets and form a circuit. In this geometry, only the central region of the filament could be thermally isolated and most of the filament was in direct contact with the diamond anvils above and below the inner gasket. As a result, the design of Zha and Bassett[65] relied on the high thermal conductivities of the diamond anvils and inner gasket material to keep the regions outside the insulated pressure chamber cool. Furthermore, the complex experimental geometry presents a significant manufacturing difficulty. The heater was able to achieve a maximum reported temperature of 2800 K, but due to the use of a non-metallic inner gasket, the achievable pressure was limited to <10 GPa. Zha *et al.*[66] reported a modified version of this design in which the non-metallic inner gasket was replaced by rhenium that was layered between the insulation layer and lower supporting gasket and had a slot cut into one side (through which the heating filament runs) to maintain electrical isolation. This modification extended the achievable pressure range to 77 GPa, but the differences in the insulation geometry and gasket material reduced the maximum temperature that could be reached to 1900 K.[66] As such, IRH designs capable of heating non-metallic samples are currently limited to 1900 K above 10 GPa, insufficient for reproducing deep lower mantle conditions.

In this article, we present a new method designed to avoid the complexities and issues described above and to achieve resistive heating of non-metallic samples at lower mantle conditions. A novel "split-gasket" design is employed, in which we cut a typical metal DAC gasket in half and place a resistive heating filament inside the pressure chamber to bridge the gap and form a circuit. This approach completely isolates the electrical filament from the diamonds, eliminates the need for a composite gasket, allows the heater to be made from commonly available materials, and maintains gasket support during compression. In contrast to previous IRH designs,[65,66] our experimental geometry is greatly simplified, enabling efficient and reproducible generation of high P–T conditions beyond the limits of other IRH designs. We believe that our new IRH-DAC design provides an important tool for investigations of materials at extreme conditions and is a significant step forward in heating techniques for the diamond anvil cell. It is particularly suited to the study of non-metallic and refractory materials, such as lower mantle minerals.

II. METHODS

A. Laser micromachining

We found it necessary to use a specialist laser micromachining system to fabricate the sub-millimeter components of the IRH experiments. All laser machining procedures were performed using an Oxford Lasers A-Series Laser Micromachining System equipped with a pulsed 1064 nm neodymium-doped yttrium orthovanadate (Nd:YVO_4) solid state laser, frequency doubled to 532 nm (Innolas NANIO 521-10-V). The nominal power output is 11.4 W at 40 kHz, with a pulse width of <30 ns and a pulse to pulse stability of <1%. The precision of the x–y stage is ~1 μm, and the focused spot size is ~3 μm. The pulse energy is 250 μJ at 40 kHz, giving a peak power of >8.3 kW.

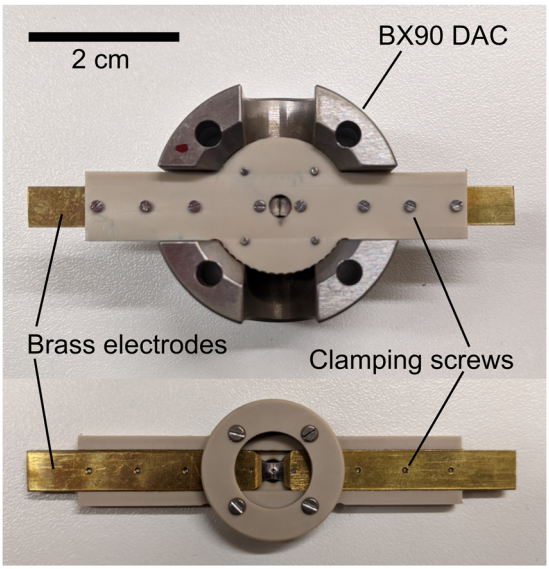

FIG. 1. Photograph of an IRH gasket holder mounted in the bottom half of a BX90 DAC along with the reverse side of the holder. The full technical drawings of the holder are available in the supplementary material.

B. IRH experimental technique

The IRH gaskets must be held in place as an experiment is prepared to avoid any relative movement between the two sides when the gasket is cut. We used reusable custom holders for this purpose (Fig. 1; schematics are also provided in the supplementary material). The holders were machined from polyether ether ketone (PEEK), a thermoplastic with excellent mechanical properties, which is resistant to temperatures up to several hundred degrees Celsius. Two brass electrodes clamp the gasket into a slot in the body of the holder and extend beyond the DAC body so that electrical connectors can be attached. The gasket holder was designed to fit tightly into a BX90 DAC[71] so that the position of the diamonds relative to the gasket remained constant as an experiment was assembled. Long rectangular gaskets were used to maximize the clamped surface area and provide a good electrical contact to the brass electrodes. We used gaskets laser cut from 250 μm thick stainless steel sheet for these experiments, but any electrically conductive material can be used (e.g., rhenium). After clamping into a holder, each gasket was pre-indented by compression in a DAC to 15 GPa, resulting in a gasket thickness of ~70 μm in the culet region. The gasket is then partially split, leaving just the culet region intact. This was achieved by milling 100 μm wide slots up to the edge of the culet on both sides using a laser milling routine designed to minimize thermal distortion near the thin culet region and the amount of conductive debris left in the slots. The slots were cleaned by flushing with acetone and then filled with a temperature resistant, non-conductive two-part epoxy (Loctite Stycast 2850FT). A circular hole with a diameter of 150 μm was then laser-drilled in the center of the culet region to form a pressure chamber to accommodate the heating filament. The electrical isolation of the two sides of the gasket was completed by laser-milling two 80 μm wide slots that extend from the central chamber to the Stycast filled slots at the edge of the culet. The culet region is cleaned with a fine needle and placed in an ultra-sonic bath with acetone to remove any debris. The resistive heating filaments were machined from 12.5 μm thick rolled rhenium foil (GoodFellow). First, a 10 μm diameter sample chamber with vertical sides was created by laser percussion drilling. Next, the filament shape was cut out around the pre-drilled hole. The "bow tie" shape of the filament was designed to maximize the area of the electrical contact between the filament and the steel gasket while creating a well-defined hot region in the center of the filament by reducing the cross-sectional area (thereby increasing resistance; Fig. 2).

Next, the experimental sample is pre-loaded into the IRH filament. We found that the simplest procedure for this is to place a small piece of sample material roughly the same size as the sample chamber directly on top of it and then use a DAC with a pair of large diameter diamonds to gently press the sample into the hole. To assemble an experiment, the gasket holder is placed in a BX90 DAC and seated on the lower anvil. The filament assembly is then placed in the central hole sandwiched between layers of Al_2O_3 that fill both the sample chamber and the slots in the culet region (Fig. 2). This material provides thermal insulation for the diamonds as well as mechanical support for the gasket so that the slots remain open as the cell is compressed. In these experiments, we used Al_2O_3 as the insulating material, but other similarly hard ceramics could be chosen to suit the experiment (such as MgO, SiO_2, or ZrO_2), provided they are unreactive with the sample at the target P–T conditions, are optically transparent, and have relatively low thermal conductivity.

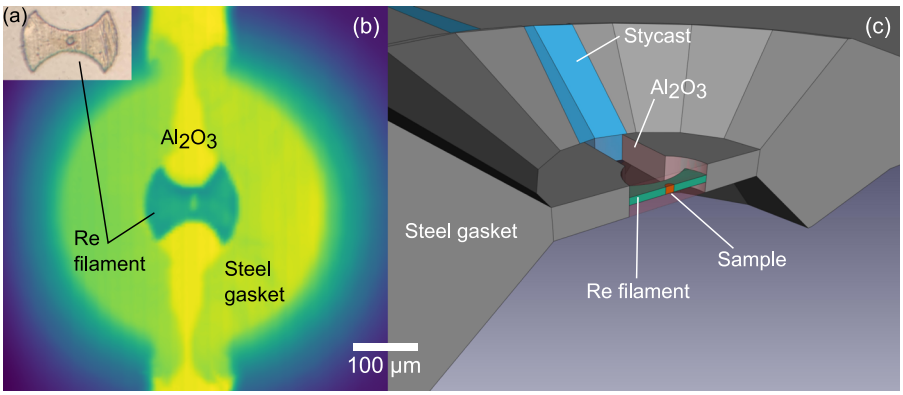

FIG. 2. (a) Photomicrograph of a rhenium IRH filament prior to loading. The sample chamber is 10 μm in diameter, and the filament thickness is 12.5 μm. (b) Synchrotron x-radiograph of experiment No. 5b showing the IRH system at pressure (17 GPa). (c) 3D CAD model showing a cross section of the IRH sample environment.

As loose alumina powder is fairly compressible and the slots need to be braced open, we pre-compressed alumina nano-powder (<50 nm, Sigma-Aldrich) into densified plates using a hydraulic hand press. These plates were then broken up into form-fitting pieces to fit into the milled region of the culet. Each filament was carefully loaded into the central hole, orientated so that it bridges the gap between the two halves of the gasket, and seated horizontally within the chamber. Careful orientation of the filament is important to avoid any rotation or shearing during compression. A small amount of loose alumina nano-powder was added along with the plates above the filament to fill in any remaining void spaces. If the sample is expected to react with the chosen insulating medium during an experiment, disks of another material that is unreactive with the sample can be placed above and below the filament to chemically isolate the sample. The only limitation is that the majority of the pressure transmitting medium must be a hard ceramics capable of maintaining the mechanical strength of the assembly.

C. Temperature generation and measurement

To illustrate the efficacy of our IRH-DAC design in performing high P–T experiments with *in situ* x-ray diffraction measurements, four cells were heated at beamline I15, Diamond Light Source, UK. After the initial heating runs, each of the cells was compressed further and reheated at a higher pressure. One of the cells was heated three times to make a total of nine experiments (Nos. 3*a*–6*b*). Two further off-line heating experiments were made in the Diamond Anvil Cell Laboratory at Bristol (No. 7*a*/*b*). The details of the experimental runs are presented in Table I.

To conduct a heating run, electrical leads were attached to the brass electrodes of the gasket holder with crocodile clips and a programmable DC power supply used to supply current. We used an Aim-TTi EX2020R 400 W power supply for experiments performed at Diamond Light Source and an Elektro-Automatik 5040-40-A power supply for experiments performed at Bristol. During experiments, the IRH-DAC was placed in a water-cooled copper jacket to ensure the gasket holder and cell itself did not suffer any thermal distortion, although any warming of the DAC body was minimal.

Temperatures during experimental runs at Diamond Light Source were measured spectroradiometrically using the system in place on the laser-heating stage at I15.[73] The system collects thermal emission from a region ~3 μm in diameter, with the aperture pre-aligned to the position of the x-ray beam (with an accuracy of ~1 μm) and periodically checked for drift throughout the experiments.[73] For experiments performed at Bristol, four-color multi-spectral imaging radiometry was used to allow us to illustrate the temperature gradients within an IRH experiment. This system has previously been described in detail by Lord and Wang.[74]

D. Synchrotron x-ray diffraction

In situ angle-dispersive x-ray powder diffraction measurements were made using an x-ray beam with a wavelength of λ = 0.4246 Å, which was micro-focused to a nominal beam dimension of 6 × 4 μm^2 (full width at half maximum) to minimize scattering from the rhenium filament surrounding the sample chamber. Diffraction patterns were collected with a Pilatus 2M detector and a typical acquisition time of 30 s. The sample to detector distance was calibrated using a CeO_2 standard. As the sample material was only present inside the sample chamber, which was similar in diameter (~10 μm) to the x-ray beam, we were able to precisely locate the sample by maximizing its XRD signal in a 2D scan across the pressure chamber, which was first located using an optical image centered on the x-ray beam. The x-ray diffraction images were integrated to one-dimensional spectra and the peaks were indexed using the *GSAS*-II software.[75] The background, fitted as a cubic spline, was subtracted from each pattern and diffraction

TABLE I. Starting materials and P–T conditions of IRH experiments.[a]

		P_{pre} (GPa)		P_{post} (GPa)		P_{max}		
Run	Sample	P_{Mo}	P_{KCl}	P_{Mo}	P_{KCl}	P_{Mo}	P_{KCl}	T_{max} (K)
No. 3*a*	KCl + Mo	3.0(1)	3.5(1)	···	···	···	< 2[b]	1167(5)
No. 3*b*	KCl + Mo	10.7(2)	···	11.9(1)	···	22.7(1)	···	2059(1)
No. 4*a*	KCl + Mo	···	4.1(0)	···	4.1(0)	···	···	<1150
No. 4*b*	KCl + Mo	···	5.1(0)	···	···	···	···	<1150
No. 5*a*	KCl + Mo	17.0(1)	···	17.7(3)	···	···	···	<1150
No. 5*b*	KCl + Mo	16.6(2)	···	25.9(4)	···	42.4(4)	39.6(3)	2002(60)
No. 5*c*	KCl + Mo	33.7(2)	30.1(8)	···	29.7(5)	64.2(2)	62.6(3)	3059(1)
		P_{Pt}		P_{Pt}				
No. 6*a*	Ti35[c] + Pt	1.6(1)		12.2(1)		20.4(3)		1941(36)
No. 6*b*	Ti35[c] + Pt	16.7(1)		26.8(1)		40.1(6)		2337(72)
		P_{Raman}						
No. 5*d*	KCl + Mo	43(1)						
No. 7*a*/*b*	Al_2O_3	25(1)						

[a]Uncertainties on P–T conditions in parentheses are 1σ on the last digit.
[b]Pressure dropped below the B1–B2 KCl transition at ~2 GPa.[72]
[c]$Ca(Si_{0.65}, Ti_{0.35})O_3$ glass.

peaks attributed to the pressure calibrants (Mo, B2 KCl, or Pt) were individually fit to pseudo-Voigt profiles using the program *fityk*.[76] Uncertainties in the peak parameters, including position, were estimated from the fitting procedure. As all of the pressure calibrants used were cubic, a lattice parameter, $a(hkl)$, was calculated directly from each present reflection and a weighted arithmetic average, $\bar{a}_m$, was used to determine unit cell volumes. Pressure was determined from the unit cell volumes of the calibrants and their known thermal equations of state.[77–79] For experiments performed at Bristol, pressure was determined from the Raman shift of the singlet peak of the diamond anvil at the culet surface using the calibration of Walter *et al.*[38]

III. RESULTS AND DISCUSSION

A. Heater performance

Our IRH-DAC design enables remarkably precise and stable power generation over the duration of long experiments. Temperatures up to 3000 K were generated within the sample chamber, with no apparent temperature limit imposed by increasing pressure, as is common with other resistive heating techniques. During initial compression, the alumina filled slots typically contracted unevenly and began to pinch at the edges of the culet, but we found that heating improved the geometry of the slots, which became increasingly parallel after heating. This allowed cells to be compressed further and

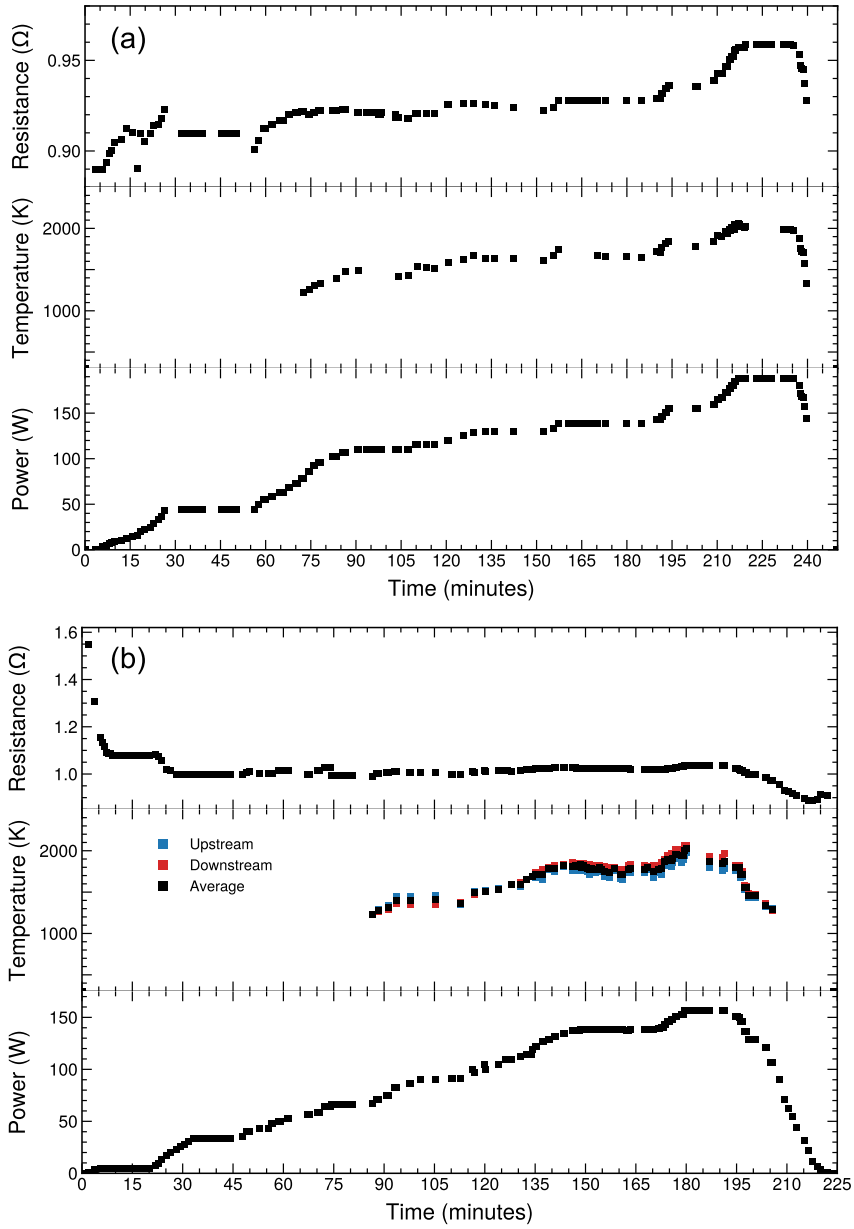

FIG. 3. Plots of electrical power, measured sample temperature, and circuit resistance over the duration of experiments (a) No. 3*b* and (b) No. 5*b*.

re-heated at higher pressures, making a large P–T region accessible with a single loading.

1. Electrical behavior

The measured resistance across the whole circuit of an IRH cell was typically ~0.9 Ω (Fig. 3). In some runs, the measured resistance prior to heating was extremely high (kΩ) or no circuit was detected with a multimeter due to poor contact between the filament and steel gasket. In all cases, this was solved by applying a current of 4 A across the circuit. This was most likely due to local heating at contact points and thermal annealing of the filament–gasket contact. The power–temperature relationship was very linear across the whole range of measured temperatures in our experiments and was in the range of 7.3–15.3 K/W (Fig. 4). This ratio was different for each run, which can be explained by slight differences in mechanical deformation of the filament during compression, variations in insulation thickness, and differences in resistivity with varying pressure between runs. The power required to achieve a given temperature is higher in the experiments reported here than those reported by Zha and Bassett[65] due to differences in the thermal conductivity and thickness of the insulation material and the geometry of the filament. Nevertheless, we successfully heated to sample temperatures of 3000 K with no damage to the diamond anvils or other components and the power required was in the normal range that commonly available power supplies can provide. The precision of commonly available programmable DC power supplies is typically ~0.1 W, giving our IRH-DAC a theoretical precision of ~1 K, which is similar to the analytical precision of spectroradiometric temperature measurements.[48] A rigorous linear relationship between power and temperature is useful as it provides the possibility to use an extrapolation from a linear regression of the power–temperature relationship to estimate temperature when no spectroradiometric temperature measurement is available or below the thermal limit of spectroradiometry. The average 95% prediction interval of the linear fits to the power–temperature relationship was 5.5% of the temperature (Fig. 4). However, the period of decreasing circuit resistance observed at the start of several experiments suggests that the linear relationship does not hold down to room temperature (Fig. 3). This is also evident from the fact that the zero power intercepts of the fits are offset from room temperature (Fig. 4). The performance of the heater in this region should be investigated further before a power–temperature calibration below 1200 K can be reliably established or deemed feasible. A spectrometer with sensitivity in the near-IR spectral range (such as an InGaAs detector) could be used to measure spectroradiometric temperature down to 500 K.[80]

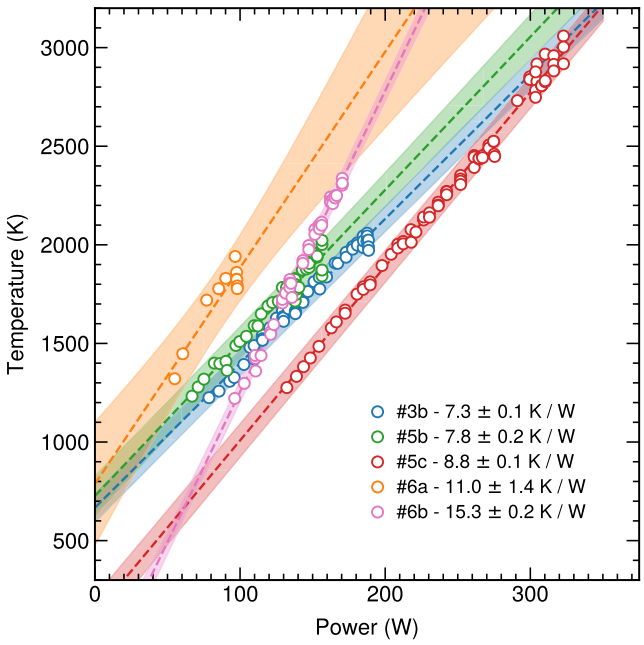

FIG. 4. Plots of sample temperature vs electrical power during temperature increase. Temperatures below ~1200 K were too low to measure with spectroradiometry. Uncertainties on individual temperature measurements were typically <1 K and are smaller than the scale of the data points. The dashed lines show linear fits to the data, and the shaded regions show 95% prediction intervals. The linear fits and 95% prediction intervals (which show where a future temperature measurement would be statistically expected to fall at a set power) have been extrapolated down to zero power to demonstrate the difficulty in using electrical power to estimate temperature below the thermal limit of spectroradiometry.

During runs where the temperature was slowly increased and decreased to and from a maximum, the temperature achieved at a set electrical power was also observed to be lower on cooling. This can also be seen as a reduction in the measured resistance of the whole circuit after heating (Fig. 3). We assume that this is due to the improvement of the contact between the gasket and filament during heating and the removal of distortion induced by cold compression. Previous studies of Joule heating inside a DAC sample chamber found that multiple temperature cycles were necessary to achieve a linear power–temperature relationship and achieve stable temperature generation,[65] but this is unnecessary with our design, and the heater appears to stabilize during the first 40 W of power application (Fig. 3).

2. Temperature stability

The resistance of the heater can change with temperature and pressure or as a result of mechanical deformation. This can lead to temperature instability over the duration of an experiment. Applying a constant current during a resistive heating experiment may lead to unstable temperature generation and even cause a run-away temperature increase. This is because the resistance of a metal filament will increase with temperature, and so more electrical power is needed to maintain the current as the temperature increases. To avoid this issue, we used a regulated constant voltage mode in experiments performed at Diamond.

During experiment No. 5*b*, we measured the temperature at a constant voltage of 11.9 V over a 20 min period, a timescale typical of a laser heating experiment. The sample temperature decreased slowly, at a constant rate of 5 K/min, while the measured resistance of the circuit remained stable, suggesting that the temperature decrease was caused by heat loss from the sample to the diamond anvils or that any decrease in electrical power was below the precision of the power supply readout. This temperature change could be easily controlled with only minor adjustments to the electrical power, as the rate is constant and slow.

To further investigate the stability of our IRH-DAC over longer time periods, and the dependency on the power supply regulation mode, we conducted two additional heating runs at Bristol using regulated constant voltage (No. 7*a*) and constant power (No. 7*b*) modes. The temperature was passively monitored, and no manual adjustments to the voltage or power were made during these experiments. In contrast to experiment No. 5*b*, the voltage control test conducted at Bristol (No. 7*a*) showed an increase in temperature over the duration of the experiment (Fig. 5). This opposite behavior could be explained by differences in the sample environment, such as insulation thickness, or by a different method of voltage regulation used by the power supply. Nevertheless, the rate of temperature change was also extremely low and could be easily controlled by compensating for the power increase, which rose 4 W over the 4 h test. Although the temperature change appears to be nonlinear, we found the behavior to be best fit by two periods of linear temperature increase—initially a rate of 1 K/min over a 30 min period, followed by a rate of 0.16 K/min for the remaining 3.5 h of the test. In a 90 min stability test of their design, Zha and Basset[65] similarly found an initial 30 min period of faster warming, which they attributed to thermal equilibration of the heater with the body of the DAC. The temperature increase during the first 30 min of their test was much greater than ours (~ 250 K), likely due to the larger heated region in their design and thermal equilibration with more thermally conductive components due to heating outside the insulated pressure chamber.[65] However, the stability test conducted by Zha and Bassett[65] was conducted in a constant current mode, which may account for some of the differences in performance.

We conducted a subsequent test using automatic power regulation that demonstrates that any average temperature change when using a constant voltage mode is a result of compensation by the power supply and is not intrinsic to our IRH-DAC design [experiment No. 7*b*, Fig. 5(b)]. After a short stabilization period of <2 min, during which the sample temperature fell by 20 K, the

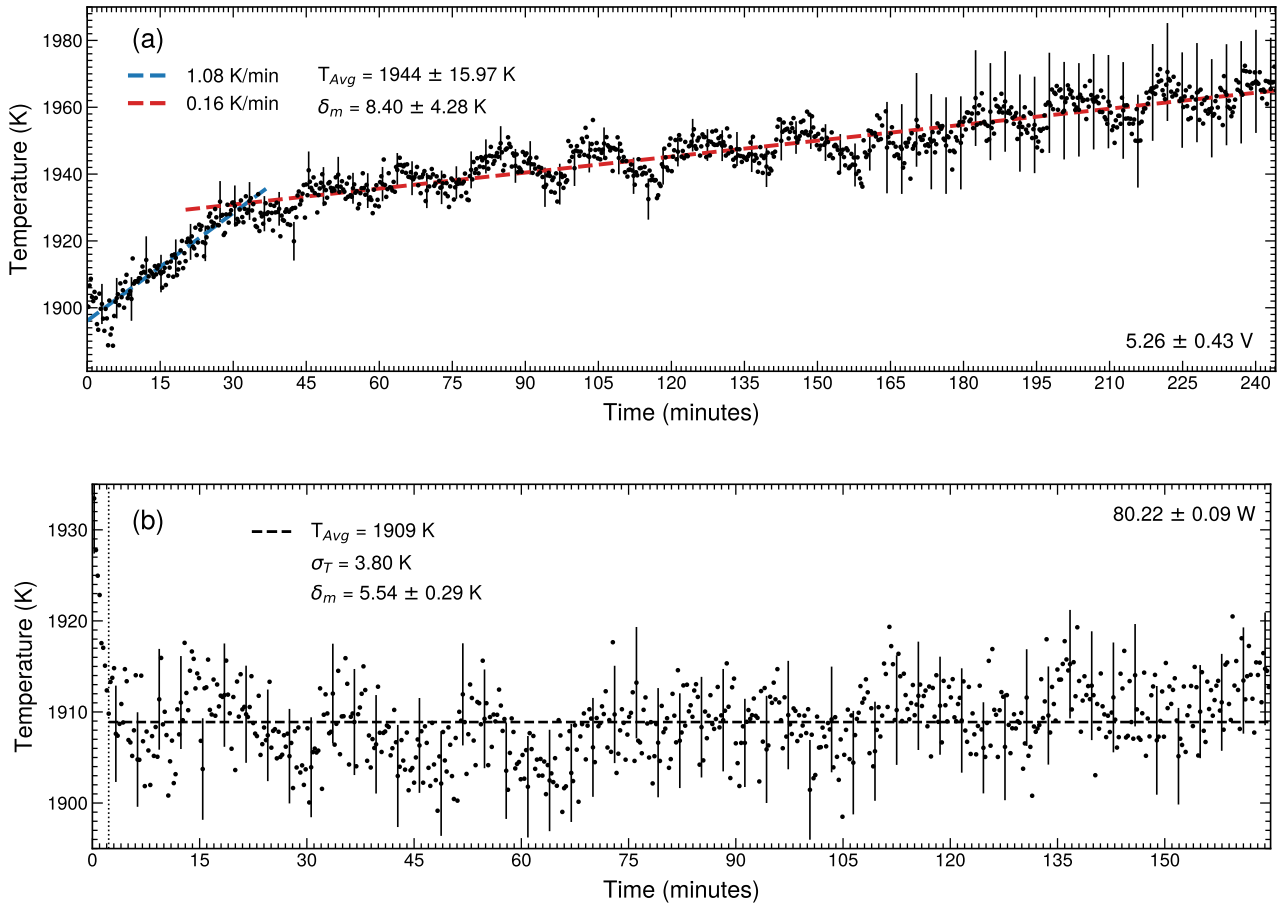

FIG. 5. (a) Sample temperature measured over a 4 h period with a constant voltage of 5.3 V. The temperature rises ~60 K over the 4 h experiment. This can be characterized as two periods of linear increase, shown by the dashed lines. (b) Sample temperature measured over a 2.75 h period with an electrical power of 80 W. A 2 min stabilization period can be observed at the start of the test. The average temperature (T_{Avg}) is 1909 K for the remainder of the test with a standard deviation (σ_T) of 3.80 K. The average measurement uncertainty (δ_m) was 5.54 ± 0.29 K. Statistical analysis suggests (with >99% certainty) that the observed scatter is stationary (Augmented Dickey–Fuller[81,82] test statistic = −4.024, p = 0.001) and is normally distributed (Shapiro–Wilk[83] test statistic = 0.998, p = 0.560). For both (a) and (b), the error bars represent 1σ uncertainty in the temperature measurement and are only plotted for every 12th measurement so that the scatter can be seen.

temperature was stationary. The average measured temperature over a period of 2.75 h was 1909 ± 3.8 K, and the standard deviation (3.8 K) was <0.2% of the temperature and smaller than the average analytical precision in the temperature measurements (5.54 ± 0.29 K). It is statistically likely that the measured temperature variation is simply a result of the analytical uncertainty on the temperature measurement as the scatter in the measured temperatures is Gaussian (Shapiro–Wilk[83] test statistic = 0.998, p = 0.560) and occurs as a stationary process with no trend (Augmented Dickey–Fuller[81,82] test statistic = −4.024, p = 0.001), although we note a slight instability in the power regulation (σ = 0.09 W), suggesting that the performance of our IRH-DAC could be increased even further by a more stable power supply. Temperature during IRH-DAC experiments using our design can therefore be controlled to an accuracy of <±10 K over the duration of long experiments lasting multiple hours. Although the stability test was stopped after nearly 3 h, there was no indication that any significant temperature fluctuations would be observed during longer experiments.

3. Quench rates

The sample was quenched at the end of experiment No. 7*b* by switching off the power supply. As the heated region is so small, this was likely to be almost instantaneous. The pressure chamber geometry remained stable, and the cell could be successfully reheated after quench. Potential applications of these rapid quench rates include the deep supercooling of molten materials to by-pass crystallization for the synthesis of novel solid-state amorphous phases at high-pressure.[9]

4. Temperature gradients

Two-dimensional temperature maps of the IRH-DAC made using four-color multi-spectral imaging radiometry illustrate the radial temperature gradients within the cell and sample chamber. The maximum measured temperature of the filament was typically ~300–400 K hotter than the sample. However, as the sample chamber is so small (~10 μm diameter) the gradients within the sample are minimal (less than 10 K/μm in the central region, but larger near the edges closest to the filament hotspots, Fig. 6). This is lower than the typical temperature gradients across a laser heating spot of a comparable size,[46] and as the entire sample is heated, there is no risk of analyzing an unheated portion of the sample. The temperature gradients along the y-axis are steeper than along the x-axis due to the location of the hotspots. The radial temperature gradients in our design appear to be slightly higher than the previous IRH design of Zha and Bassett.[65] Zha and Bassett[65] reported a difference of 51 K between a temperature measured in the center of the sample and at a point near the edge of the sample chamber, whereas the difference (in the same direction) measured in experiment No. 5*d* was ~80 K (Fig. 6). This is because of the smaller heated region in our design. Nevertheless, the temperature variation across the whole analyzed volume will determine the temperature uncertainty in scattering measurements. The standard deviation of temperature across the sample volume in our experiments was <35 K (Fig. 6). The radial temperature gradients could also be reduced by future refinement of the filament shape. The temperature gradients in the axial direction are not measured but are likely to be lower than those in an equivalent laser heating experiment. This is because heat is generated internally throughout the filament thickness, unlike a laser heating experiment where the laser power is absorbed at the surface.[84] The average difference in measured temperature based on the radiation from the sample surface on either side of the cell was 31 K for runs performed at Diamond, although this rose to a maximum of 86 K in experiment No. 6*b*. This is due to differences in the thickness of insulation on either side of the filament and could be improved by laser milling form-fitting pieces of single crystal insulation to an exact and equal thickness. Reduced temperature gradients will also lead to reduced thermal pressure gradients, which in the laser heated DAC can reach 1 GPa/μm.[85]

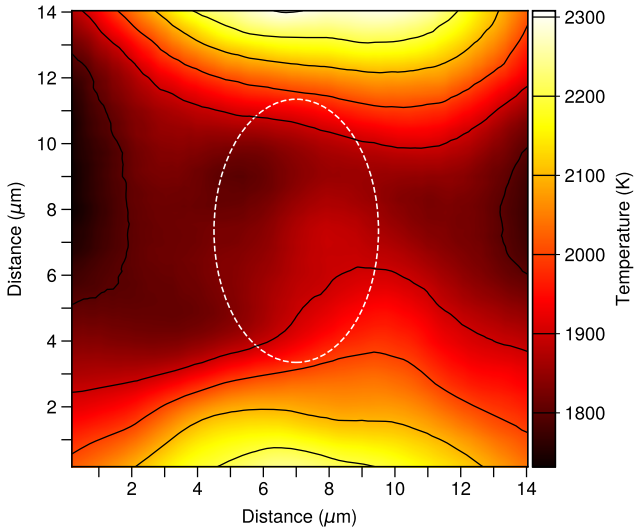

FIG. 6. 2D temperature map of an IRH heating experiment (No. 5*d*) made using four-color imaging radiometry. The pressure prior to heating was ~43 GPa. The dashed white line shows the outline of the sample chamber, which had compressed and deformed during previous runs. The mean temperature inside the sample region was 1872 ± 34 K, although the absolute range of temperatures inside the sample chamber was 178 K. The filament hotspots on either side of the sample chamber are typically 300–400 K hotter than the sample.

B. X-ray diffraction

During nine heating experiments, we were able to obtain *in situ* XRD measurements across a large P–T range that would otherwise only be accessible with laser heating (Table I, Fig. 7). This shows that our IRH-DAC is not only capable of performing long stable heating experiments at lower mantle conditions but is a useful tool for rapid acquisition of the high-resolution P–V–T datasets required for constraining the thermoelastic parameters of minerals in the deep Earth. One of the heated cells (No. 6*a*/*b*) was loaded with glass with the stoichiometric composition $Ca(Si_{0.65}, Ti_{0.35})O_3$, which should form a stable perovskite phase at P > 10 GPa and T > 1500 K.[86] Titanium bearing calcium perovskite is likely to be an important phase in the lower mantle, and its physical properties are relevant to the interpretation of inclusions found in "super-deep" diamonds, the seismic structure of the deep Earth, and the freezing of magma oceans present during early Earth history.[35,87,88] Figure 8 shows a contoured waterfall plot of patterns collected during experiment Nos. 6*a* and 6*b*. Corundum peaks can be seen to

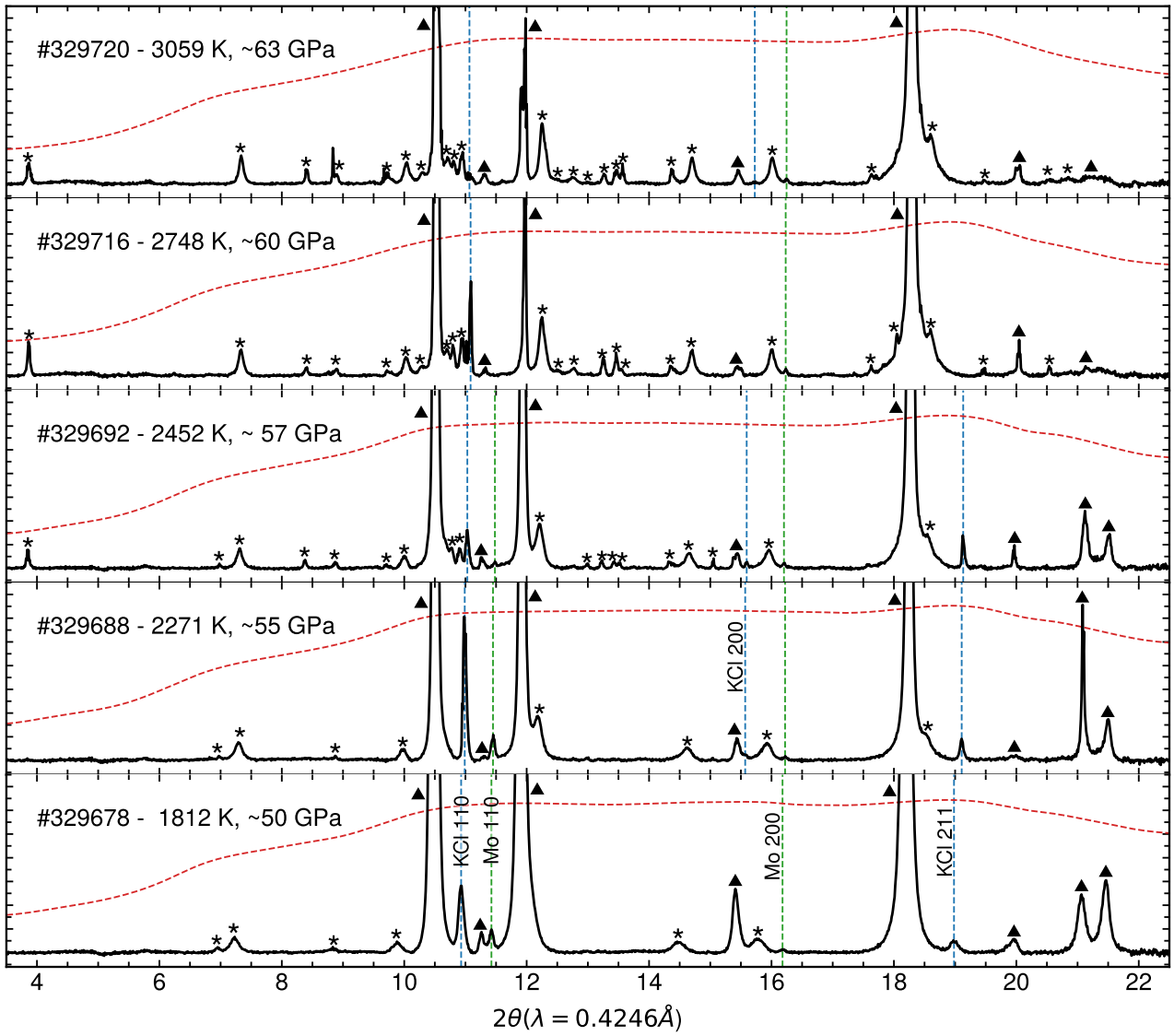

FIG. 7. Representative 1D background-subtracted XRD spectra from experiment No. 5c. The subtracted backgrounds are shown by the dashed lines (red). The vertical dashed lines show refined peak centers of pseudo-Voigt fits to KCl (blue) and Mo (green) peaks. The peaks attributed to Al_2O_3 are denoted by asterisks (∗) and rhenium by triangles (▲). The signal-to-noise ratio of sample peaks was reduced at higher temperatures due to grain growth, which resulted in "spottier" diffraction patterns.

appear during initial heating as the alumina nano-powder recrystallizes. Sample peaks appear from 1450 K as the $Ca(Si_{0.65}, Ti_{0.35})O_3$ glass begins to crystallize and remain present in all further diffraction patterns. The sample peaks can be explained by an orthorhombic unit cell with space group *Pbnm* as expected for this composition. However, refinement of the unit cell yielded lattice parameters $a = 4.57(1)$, $b = 4.32(1)$, and $c = 6.56(1)$ at 12.2 GPa (run No. 6*a*) and $a = 4.51(1)$, $b = 4.27(1)$, and $c = 6.47(1)$ at 26.8 GPa (run No. 6*b*) after quenching to room temperature, which gives volumes that are much lower than expected at these pressures.[35,86] This is probably due to a reaction with the alumina pressure medium. The effect of thermal pressure during the experiments is apparent as peaks shift toward higher 2θ angles during heating (Fig. 8).

1. Thermal pressure and nonhydrostaticity

An increase in pressure during heating is inevitable in a volumetrically constrained sample chamber. As a result, pressure should be monitored during experiments. We found a near-linear pressure dependency on temperature, with a typical increase of 0.5–1 GPa/100 K. Total thermal pressure during experiments was 50%–100% of the pressure measured after heating. IRH experiments differ from laser heating experiments in that the sample is heated from the outside, rather than from within. The thermal expansion

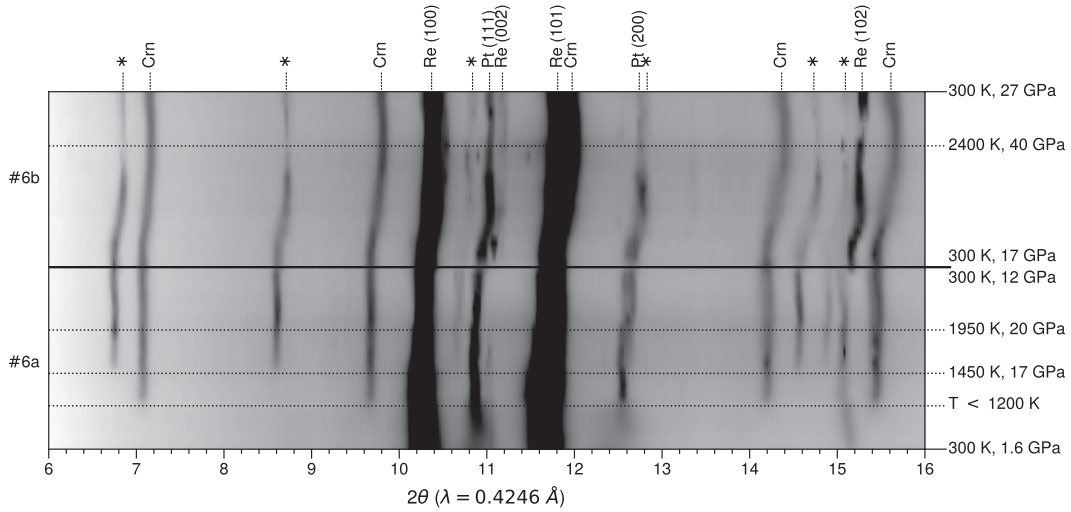

FIG. 8. Contoured waterfall plot of 1D x-ray diffraction patterns collected during experiment Nos. 6*a* and 6*b*. The peaks attributed to Pt, Re, corundum (Crd), and the sample (*) are indicated, as are *P*–*T* conditions of selected patterns throughout the experiments.

of the filament surrounding the sample compresses the sample as the experiment is heated. This is consistent with our observation of a linear reduction in unit cell volume as a function of temperature (unit cell volume data can be found in the supplementary material). Some changes in pressure will also result from the thermal relaxation of the IRH assembly. Pressures measured after heating were higher than those measured prior to heating (Table I, Fig. 9).

Pressures in the DAC commonly deviate from hydrostatic, as uniaxial compression can increase the differential stress, t, between the axial and radial directions. Soft or fluid pressure transmitting media are commonly used to reduce the differential stress in DAC experiments;[89] however, the IRH-DAC design relies on a very incompressible pressure medium to keep the cell geometry stable. As non-hydrostatic stress affects each (hkl) reflection to a varying degree, the axial stress condition, t, can be estimated from a "gamma plot"—a plot of the measured lattice parameters for a given reflection, $a_m(hkl)$, against $3\left(1-3\sin^2\theta\right)\Gamma(hkl)$, where θ is the diffraction angle and $\Gamma(hkl) = \left(h^2k^2+k^2l^2+l^2h^2\right)/\left(h^2+k^2+l^2\right)^2$.[90] The St value is derived from the intercept (M_0) and slope (M_1) of the gamma plot: $St = -3M_1/M_0$, where S is the single crystal elastic compliance: $S = (S_{11} - S_{12} - S_{44}/2)$. As only two or three reflections from each pressure calibrant were present in the diffraction patterns (Fig. 7), gamma plots were only made when the (200) reflection was present, which is most sensitive to deviatoric stress for cubic materials in DAC experiments.[91,92] The elastic anisotropy of Pt and Mo under pressure was calculated from data available in the literature,[93,94] and t was calculated for experiments before and after heating (Table II). As S of B2 KCl under pressure and S of Pt and Mo at high temperature are not available, the St value was used as a stress indicator for all other experiments and during heating runs. The measured t of Pt in experiment Nos. 6*a* and 6*b* was less than 1.5 GPa after heating (Table II), which is comparable to cold compression in a neon pressure medium (t = 1–4 GPa in Ref. 92) and only slightly elevated compared to laser annealed samples in NaCl (t < 1 GPa in Ref. 95). The axial stress is noticeably lower after heating due to thermal annealing and relaxation in the pressure chamber. A reversible component to the change in axial stress was also observed during heating (Fig. 10). St was observed to decrease with temperature and in many runs became negative.

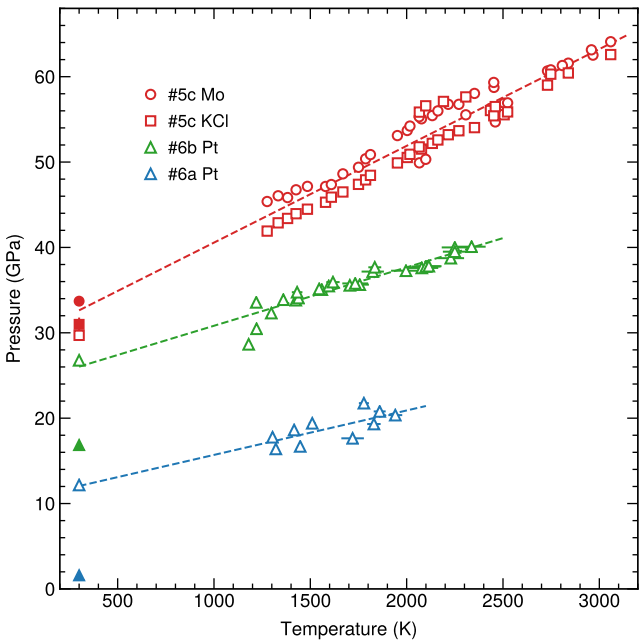

FIG. 9. Plots of the dependency of pressure on temperature in our IRH-DAC for experiment Nos. 5*c*, 6*b*, and 6*a*. The closed symbols show pressures measured prior to heating. The dashed lines show linear fits to the data.

TABLE II. Axial stress (t) and pressure (P) before and after heating.[a]

		Pre-heating		Post-heating	
Run	Calibrant	P (GPa)	t (GPa)	P (GPa)	t (GPa)
No. 5*a*	Mo	17.02(7)	3.24(0)	17.66(30)	−2.72(3)
No. 5*b*	Mo	16.60(19)	−4.12(3)	25.86(39)	···
No. 5*c*	Mo	33.71(18)	−1.35(1)	29.70(52)	···
No. 6*a*	Pt	1.61(8)	6.83(1)	12.17(6)	1.42(0)
No. 6*b*	Pt	16.86(6)	−1.24(0)	26.78(7)	−0.72(0)
			St		*St*
No. 3*a*	KCl	3.55(6)	−0.0008	···	···
No. 4*a*	KCl	4.09(1)	0.0052	4.07(1)	0.0007
No. 4*b*	KCl	5.12(2)	0.0381	···	···

[a]Uncertainties in parentheses are on the last digit and are 1σ.

Negative axial stress (where the radial stress component, σ_3, is larger than the axial stress component, σ_1) has been observed in diamond anvil cell experiments with highly compressible pressure media and is attributed to the radial collapse of the sample chamber.[91] In our experiments, it is likely that the additional hard components (i.e., the filament) within the pressure chamber impose radial pressure on the sample as they thermally expand during heating. This appears to have the effect of counteracting some of the axial stress caused by the uniaxial compression of the DAC and likely results in lower axial stress than laser heating experiments performed with a similarly hard pressure medium.

For experiments loaded with two calibrants, we observed a systematic offset between pressures measured from the volume of Mo and from the volume of KCl. The offset was present down to room temperature, so is not only a thermal effect, and was noticeable in post-heating pressures with low measured t, so is unlikely to be a result of deviatoric stress in the sample chamber. Although the estimated uncertainty on our pressure measurements using Mo and KCl calibrants do not overlap, the true uncertainty is likely to be much larger as studies reporting equations of state typically do not publish the full covariance matrix required to propagate the uncertainty in fitted parameters, which arises from scatter in the P–V–T dataset. There are several sources that can introduce uncertainty or systematic errors to an equation of state, including its analytical form, the choice of pressure scale, and most importantly, measurement uncertainty in the P–V–T dataset, with temperature being the largest contributor. Temperature uncertainty is important even in studies of processes that are relatively insensitive to temperature (e.g., mapping phase boundaries with very low Clapeyron slopes) because the error in pressure is largely dependent on the error in temperature due to its much higher relative uncertainty compared to the uncertainty in the volumetric measurement of the pressure calibrant. New techniques, such as our IRH-DAC design, that can reduce the temperature uncertainty in high pressure experiments are therefore key to improving our understanding of the physical and chemical characteristics of the deep Earth.

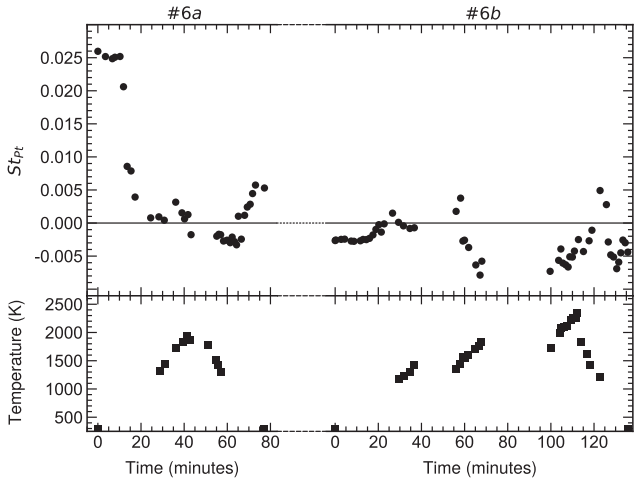

FIG. 10. Stress indicator values, *St*, of Pt derived from gamma plots for experiment Nos. 6*a* and 6*b* along with measured temperature plotted as a function of experiment duration.

C. Potential improvements

Our "split gasket" approach provides a simple design framework for performing IRH experiments. In the present study, we have demonstrated its efficacy with a 150 μm "bow-tie" Re filament, an ~10 μm diameter sample chamber, an Al_2O_3 nano-powder pressure medium/thermal insulation, and 500 μm culet diameter anvils to P–T conditions of ~3000 K and ~60 GPa. However, as the filament material/shape and insulation material/geometry are not the limiting features of the design, our IRH technique could be improved by refinement of these components. The use of different filament materials may improve the heater performance, and alternative materials for thermal insulation may improve temperature homogeneity and/or stability. Finite element modeling could help quantify the thermal gradients along the compression axis and inform refinement of the filament shape to reduce both axial and radial temperature gradients. Thermal gradients and heating efficiency are strongly controlled by the insulation geometry. More advanced micro-fabrication techniques such as femto-second laser micromachining[96,97] or xenon plasma focused ion beam milling (Xe^+-FIB)[98] will allow fabrication of form-fitting single crystal insulation, reducing axial gradients by ensuring equal insulation thickness on either side of the filament. Form-fitting pieces of insulation with a milled depression to hold the filament could also improve the efficiency of the loading procedure, potentially allowing the sample, filament, and insulation components to be assembled outside the cell and loaded into the pressure chamber as a single piece. Disks of a material unreactive with the sample could be incorporated into the design above and below the filament to chemically isolate the sample from the insulation material if necessary. Precisely milled annuli placed above and below the central portion of the filament would also allow for gas loading of a fluid pressure medium around the sample chamber itself. The pressures reached in this study (up to ~63 GPa) were limited by the relatively large culet diameter of the diamonds used (500 μm in the highest pressure run), which is itself limited by the size of the heating filament and diameter of the pressure chamber (150 μm). It is likely that smaller anvils down to ~300 μm in diameter could be used with little or no adaption of the heating filament to extend the pressure range to ~80 GPa.[99] Extending the

pressure range further is conceivable but would require further miniaturization of the filament and sample assembly. In this study, we used spectroradiometric temperature measurement in the visible range, which limited the minimum measurable temperature to ~1200 K. The use of an InGaAs detector sensitive to near-IR radiation would extend the temperature measurement range down to 500 K.[80] The full isolation of the heating filament enabled by our novel "split-gasket" approach significantly extends the P–T range accessible to IRH techniques and improves temperature stability. However, because the shorter filament must also be narrower to compensate for the reduction in resistance, the sample chamber in our design is smaller in diameter compared to previous IRH designs.[65,66] The small diameter of the sample chamber (~10 μm) in our design presents the possible issue of unwanted scattering by the filament material adversely affecting diffraction data. The diameter of the sample chamber could be increased by using a correspondingly thinner filament in future studies. Nevertheless, we were able to obtain usable XRD data using an uncollimated micro-focused x-ray beam ($6 \times 4\ \mu m^2$ full width at half maximum) in this study. Our IRH technique is ideally placed to exploit the outstanding coherence properties and sub-micron focusing of x-ray beams at fourth-generation synchrotron sources being developed now, increasing data quality and the range of techniques with which it can be interfaced.[100,101]

IV. CONCLUSIONS

Our new IRH-DAC design significantly extends the P–T range accessible to resistive heating techniques, easily encompassing the mantle geotherm to 1500 km depth. The temperature range of our IRH design is also sufficient to recreate the conditions of a hotter Archean mantle.[102] While recent advances have been made in MAP techniques, our IRH-DAC design provides a much more accessible alternative for performing resistive heating experiments at lower mantle conditions. The "split-gasket" approach adopted in our IRH design provides several benefits over existing IRH techniques applicable to non-metallic samples:[65,66] The experimental design is much simpler, and the geometry allows for the heating filament to be completely isolated within the insulated pressure chamber. These features enable more reproducible, efficient, and routine generation of high P–T conditions beyond the limits of other IRH designs. Our IRH-DAC technique is cost effective and time efficient. Fabrication of the filament and gasket geometry requires a precise laser mill, and a programmable DC power supply is needed for heating, but no other specialist equipment is required and the materials used are commonly available and relatively cheap. It takes under two days to prepare the experiments, with most of that time required for the epoxy glue to cure, and a single cell can be reheated at several different pressures for efficient data collection over a large P–T range. We also found the experiment failure rate of our IRH design to be remarkably low (with no diamonds broken during the runs performed at Diamond Light Source) in comparison to experiments pushing the limits of MAP techniques, where "blow-outs" of the expensive WC or sintered diamond cubes are common.[40] Our IRH-DAC design provides an important new tool for investigating materials at extreme conditions. The excellent temperature stability during experiments lasting many hours, reduced thermal gradients, elimination of the requirement for a metallic absorber to be mixed with the sample, and precise temperature control are significant improvements over laser heating techniques in this P–T range. These advantages make our IRH-DAC design well suited for studies requiring stable homogeneous heating, including the collection of high-resolution, accurate P–V–T data, the precise demarcation of phase boundaries, making liquid state measurements of wholly molten samples, and heating experiments over the long acquisition times required for techniques such as Brillouin spectroscopy and IXS. Our IRH-DAC technique is ideally placed to exploit the highly coherent nano-focused x-ray beams in development at current and next-generation synchrotron sources.

SUPPLEMENTARY MATERIAL

See the supplementary material for full technical drawings of the IRH holder and gasket and for plots of electrical power, sample temperature, and circuit resistance as well as plots of stress indicator values (St) for all other experiment runs. Electrical power, temperature, and pressure calibrant unit cell volume data are also provided in the supplementary material.

ACKNOWLEDGMENTS

This work was funded by the NERC under Grant No. NE/P002951/1. The authors acknowledge the additional support from NERC Grant No. NE/M000419/1. The authors also acknowledge Diamond Light Source for time on I15 under Proposal No. CY21972. O.T.L. would like to acknowledge the support from the Royal Society in the form of a University Research Fellowship (No. UF150057). B.J.H. would like to acknowledge the support in the form of a studentship awarded as part of Royal Society Grant No. RG160631 awarded to O.T.L. We would also like to thank D. Hawley, G. Mwale, and L. Breeze for their technical assistance during the development stage and C. Gregson for assistance during synchrotron beamtime at DLS.

DATA AVAILABILITY

The data that support the findings of this study are available from the corresponding author upon reasonable request.

REFERENCES

[1] L. Henry, M. Mezouar, G. Garbarino, D. Sifré, G. Weck, and F. Datchi, Nature **584**, 382 (2020).
[2] H. Tanaka, J. Chem. Phys. **153**, 130901 (2020).
[3] F. Walton, J. Bolling, A. Farrell, J. MacEwen, C. D. Syme, M. G. Jiménez, H. M. Senn, C. Wilson, G. Cinque, and K. Wynne, J. Am. Chem. Soc. **142**, 7591 (2020).
[4] Y. Akahama, H. Kawamura, D. Häusermann, M. Hanfland, and O. Shimomura, Phys. Rev. Lett. **74**, 4690 (1995).
[5] R. P. Dias and I. F. Silvera, Science **355**, 715 (2017).
[6] M. Millot, S. Hamel, J. R. Rygg, P. M. Celliers, G. W. Collins, F. Coppari, D. E. Fratanduono, R. Jeanloz, D. C. Swift, and J. H. Eggert, Nat. Phys. **14**, 297 (2018).
[7] E. Snider, N. Dasenbrock-Gammon, R. McBride, M. Debessai, H. Vindana, K. Vencatasamy, K. V. Lawler, A. Salamat, and R. P. Dias, Nature **586**, 373 (2020).
[8] D. Laniel, B. Winkler, T. Fedotenko, A. Pakhomova, S. Chariton, V. Milman, V. Prakapenka, L. Dubrovinsky, and N. Dubrovinskaia, Phys. Rev. Lett. **124**, 216001 (2020).
[9] J. W. E. Drewitt, F. Turci, B. J. Heinen, S. G. Macleod, F. Qin, A. K. Kleppe, and O. T. Lord, Phys. Rev. Lett. **124**, 145501 (2020).

[10]Q. Huang, D. Yu, B. Xu, W. Hu, Y. Ma, Y. Wang, Z. Zhao, B. Wen, J. He, Z. Liu, and Y. Tian, Nature **510**, 250 (2014).
[11]V. L. Solozhenko, V. Bushlya, and J. Zhou, J. Appl. Phys. **126**, 075107 (2019).
[12]M. Bykov, S. Chariton, H. Fei, T. Fedotenko, G. Aprilis, A. V. Ponomareva, F. Tasnádi, I. A. Abrikosov, B. Merle, P. Feldner, S. Vogel, W. Schnick, V. B. Prakapenka, E. Greenberg, M. Hanfland, A. Pakhomova, H.-P. Liermann, T. Katsura, N. Dubrovinskaia, and L. Dubrovinsky, Nat. Commun. **10**, 2994 (2019).
[13]H. Wang, M. Yu, Y. Wang, Z. Feng, Y. Wang, X. Lü, J. Zhu, Y. Ren, and C. Liang, J. Power Sources **401**, 111 (2018).
[14]Y. Huang, Y. He, H. Sheng, X. Lu, H. Dong, S. Samanta, H. Dong, X. Li, D. Y. Kim, H.-K. Mao, Y. Liu, H. Li, H. Li, and L. Wang, Natl. Sci. Rev. **6**, 239 (2019).
[15]B. Cheng, H. Lou, A. Sarkar, Z. Zeng, F. Zhang, X. Chen, L. Tan, K. Glazyrin, H.-P. Liermann, J. Yan, L. Wang, R. Djenadic, H. Hahn, and Q. Zeng, Mater. Today Adv. **8**, 100102 (2020).
[16]D. Tomasino, M. Kim, J. Smith, and C.-S. Yoo, Phys. Rev. Lett. **113**, 205502 (2014).
[17]H. Wang, M. I. Eremets, I. Troyan, H. Liu, Y. Ma, and L. Vereecken, Sci. Rep. **5**, 13239 (2015).
[18]M. Guerain, J. Pharm. Sci. **109**, 2640 (2020).
[19]X. Dong, A. R. Oganov, A. F. Goncharov, E. Stavrou, S. Lobanov, G. Saleh, G.-R. Qian, Q. Zhu, C. Gatti, V. L. Deringer, R. Dronskowski, X.-F. Zhou, V. B. Prakapenka, Z. Konôpková, I. A. Popov, A. I. Boldyrev, and H.-T. Wang, Nat. Chem. **9**, 440 (2017).
[20]B. Li, Y. Ding, D. Y. Kim, R. Ahuja, G. Zou, and H.-K. Mao, Proc. Natl. Acad. Sci. U. S. A. **108**, 18618 (2011).
[21]M. Zaghoo and I. F. Silvera, Proc. Natl. Acad. Sci. U. S. A. **114**, 11873 (2017).
[22]T. Fedotenko, L. Dubrovinsky, G. Aprilis, E. Koemets, A. Snigirev, I. Snigireva, A. Barannikov, P. Ershov, F. Cova, M. Hanfland, and N. Dubrovinskaia, Rev. Sci. Instrum. **90**, 104501 (2019).
[23]H. Nakao, M. Einaga, M. Sakata, M. Kitagaki, K. Shimizu, S. Kawaguchi, N. Hirao, and Y. Ohishi, J. Phys. Soc. Jpn. **88**, 123701 (2019).
[24]V. N. Robinson and A. Hermann, J. Phys.: Condens. Matter **32**, 184004 (2020).
[25]P. Loubeyre, F. Occelli, and P. Dumas, Nature **577**, 631 (2020).
[26]S. T. Weir, A. C. Mitchell, and W. J. Nellis, Phys. Rev. Lett. **76**, 1860 (1996).
[27]E. Sugimura, T. Komabayashi, K. Ohta, K. Hirose, Y. Ohishi, and L. S. Dubrovinsky, J. Chem. Phys. **137**, 194505 (2012).
[28]C. Liu, H. Gao, A. Hermann, Y. Wang, M. Miao, C. J. Pickard, R. J. Needs, H.-T. Wang, D. Xing, and J. Sun, Phys. Rev. X **10**, 021007 (2020).
[29]A. Ricolleau, J.-P. Perrillat, G. Fiquet, I. Daniel, J. Matas, A. Addad, N. Menguy, H. Cardon, M. Mezouar, and N. Guignot, J. Geophys. Res.: Solid Earth **115**, B08202, https://doi.org/10.1029/2009jb006709 (2010).
[30]S. M. Dorfman, in *Deep Earth: Physics and Chemistry of the Lower Mantle and Core*, American Geophysical Union (AGU) Geophysical Monograph Series Vol. 217, edited by H. Terasaki and R. A. Fischer (John Wiley & Sons, 2016), Chap. 19, pp. 241–252.
[31]C. Xu and T. Inoue, Minerals **9**, 559 (2019).
[32]H. Marquardt and A. R. Thomson, Nat. Rev. Earth Environ. **1**, 455 (2020).
[33]S. W. French and B. Romanowicz, Nature **525**, 95 (2015).
[34]A. Kurnosov, H. Marquardt, D. J. Frost, T. B. Ballaran, and L. Ziberna, Nature **543**, 543 (2017).
[35]A. R. Thomson, W. A. Crichton, J. P. Brodholt, I. G. Wood, N. C. Siersch, J. M. R. Muir, D. P. Dobson, and S. A. Hunt, Nature **572**, 643 (2019).
[36]H. Tkalčić, M. Young, J. B. Muir, D. R. Davies, and M. Mattesini, Sci. Rep. **5**, 18416 (2015).
[37]A. K. McNamara, E. J. Garnero, and S. Rost, Earth Planet. Sci. Lett. **299**, 1 (2010).
[38]M. J. Walter, A. R. Thomson, W. Wang, O. T. Lord, J. Ross, S. C. McMahon, M. A. Baron, E. Melekhova, A. K. Kleppe, and S. C. Kohn, Chem. Geol. **418**, 16 (2015).
[39]R. C. Liebermann, High Pressure Res. **31**, 493 (2011).
[40]T. Ishii, Z. Liu, and T. Katsura, Engineering **5**, 434 (2019).
[41]D. Yamazaki, E. Ito, T. Yoshino, N. Tsujino, A. Yoneda, H. Gomi, J. Vazhakuttiyakam, M. Sakurai, Y. Zhang, Y. Higo, and Y. Tange, C. R. Geosci. **351**, 253 (2019).
[42]Y. Tange, T. Irifune, and K.-I. Funakoshi, High Pressure Res. **28**, 245 (2008).
[43]D. Yamazaki, E. Ito, T. Yoshino, N. Tsujino, A. Yoneda, X. Guo, F. Xu, Y. Higo, and K. Funakoshi, Phys. Earth Planet. Inter. **228**, 262 (2014).
[44]T. Kunimoto, T. Irifune, Y. Tange, and K. Wada, High Pressure Res. **36**, 97 (2016).
[45]R. Sinmyo and K. Hirose, Phys. Earth Planet. Inter. **180**, 172 (2010).
[46]S. Anzellini and S. Boccato, Crystals **10**, 459 (2020).
[47]A. Kurnosov, H. Marquardt, L. Dubrovinsky, and V. Potapkin, C. R. Geosci. **351**, 280 (2019).
[48]M. J. Walter and K. T. Koga, Phys. Earth Planet. Inter. **143-144**, 541 (2004).
[49]O. T. Lord, E. T. H. Wann, S. A. Hunt, A. M. Walker, J. Santangeli, M. J. Walter, D. P. Dobson, I. G. Wood, L. Vočadlo, G. Morard *et al.*, Phys. Earth Planet. Inter. **233**, 13 (2014).
[50]V. B. Prakapenka, A. Kubo, A. Kuznetsov, A. Laskin, O. Shkurikhin, P. Dera, M. L. Rivers, and S. R. Sutton, High Pressure Res. **28**, 225 (2008).
[51]E. Ohtani, K. Mibe, T. Sakamaki, S. Kamada, S. Takahashi, H. Fukui, S. Tsutsui, and A. Q. R. Baron, Russ. Geol. Geophys. **56**, 190 (2015).
[52]I. Ohira, M. Murakami, S. Kohara, K. Ohara, and E. Ohtani, Prog. Earth Planet. Sci. **3**, 18 (2016).
[53]N. Dubrovinskaia and L. Dubrovinsky, Rev. Sci. Instrum. **74**, 3433 (2003).
[54]Z. Jenei, H. Cynn, K. Visbeck, and W. J. Evans, Rev. Sci. Instrum. **84**, 095114 (2013).
[55]M. Louvel, J. W. E. Drewitt, A. Ross, R. Thwaites, B. J. Heinen, D. S. Keeble, C. M. Beavers, M. J. Walter, and S. Anzellini, J. Synchrotron Radiat. **27**, 529 (2020).
[56]J. Immoor, H. Marquardt, L. Miyagi, S. Speziale, S. Merkel, I. Schwark, A. Ehnes, and H.-P. Liermann, Rev. Sci. Instrum. **91**, 045121 (2020).
[57]A. S. J. Méndez, H. Marquardt, R. J. Husband, I. Schwark, J. Mainberger, K. Glazyrin, A. Kurnosov, C. Otzen, N. Satta, J. Bednarcik *et al.*, Rev. Sci. Instrum. **91**, 073906 (2020).
[58]L.-G. Liu and W. A. Bassett, J. Geophys. Res. **80**, 3777, https://doi.org/10.1029/jb080i026p03777 (1975).
[59]R. Boehler, Geophys. Res. Lett. **13**, 1153, https://doi.org/10.1029/gl013i011p01153 (1986).
[60]R. Boehler, M. Nicol, C. S. Zha, and M. L. Johnson, Physica B+C **139-140**, 916 (1986).
[61]L. Dubrovinsky, N. Dubrovinskaia, O. Narygina, I. Kantor, A. Kuznetzov, V. B. Prakapenka, L. Vitos, B. Johansson, A. S. Mikhaylushkin, S. I. Simak, and I. A. Abrikosov, Science **316**, 1880 (2007).
[62]T. Komabayashi, Y. Fei, Y. Meng, and V. Prakapenka, Earth Planet. Sci. Lett. **282**, 252 (2009).
[63]R. Sinmyo, K. Hirose, and Y. Ohishi, Earth Planet. Sci. Lett. **510**, 45 (2019).
[64]S. Suehiro, T. Wakamatsu, K. Ohta, K. Hirose, and Y. Ohishi, High Pressure Res. **39**, 579 (2019).
[65]C.-S. Zha and W. A. Bassett, Rev. Sci. Instrum. **74**, 1255 (2003).
[66]C.-S. Zha, K. Mibe, W. A. Bassett, O. Tschauner, H.-K. Mao, and R. J. Hemley, J. Appl. Phys. **103**, 054908 (2008).
[67]L. Dubrovinsky, H. Annersten, N. Dubrovinskaia, F. Westman, H. Harryson, O. Fabrichnaya, and S. Carlson, Nature **412**, 527 (2001).
[68]N. Dubrovinskaia and L. Dubrovinsky, *Advances in High-Pressure Technology for Geophysical Applications* (Elsevier, 2005), Chap. 25, pp. 487–501.
[69]H. Inoue, S. Suehiro, K. Ohta, K. Hirose, and Y. Ohishi, Earth Planet. Sci. Lett. **543**, 116357 (2020).
[70]H. Ozawa, S. Tateno, L. Xie, Y. Nakajima, N. Sakamoto, S. I. Kawaguchi, A. Yoneda, and N. Hirao, High Pressure Res. **38**, 120 (2018).
[71]I. Kantor, V. Prakapenka, A. Kantor, P. Dera, A. Kurnosov, S. Sinogeikin, N. Dubrovinskaia, and L. Dubrovinsky, Rev. Sci. Instrum. **83**, 125102 (2012).
[72]C. W. F. T. Pistorius, J. Phys. Chem. Solids **26**, 1543 (1965).
[73]S. Anzellini, A. K. Kleppe, D. Daisenberger, M. T. Wharmby, R. Giampaoli, S. Boccato, M. A. Baron, F. Miozzi, D. S. Keeble, A. Ross, S. Gurney, J. Thompson, G. Knap, M. Booth, L. Hudson, D. Hawkins, M. J. Walter, and H. Wilhelm, J. Synchrotron Radiat. **25**, 1860 (2018).
[74]O. T. Lord and W. Wang, Rev. Sci. Instrum. **89**, 104903 (2018).

[75]B. H. Toby and R. B. Von Dreele, J. Appl. Crystallogr. **46**, 544 (2013).
[76]M. Wojdyr, J. Appl. Crystallogr. **43**, 1126 (2010).
[77]P. I. Dorogokupets and A. Dewaele, High Pressure Res. **27**, 431 (2007).
[78]K. D. Litasov, P. I. Dorogokupets, E. Ohtani, Y. Fei, A. Shatskiy, I. S. Sharygin, P. N. Gavryushkin, S. V. Rashchenko, Y. V. Seryotkin, Y. Higo *et al.*, J. Appl. Phys. **113**, 093507 (2013).
[79]S. Tateno, T. Komabayashi, K. Hirose, N. Hirao, and Y. Ohishi, Am. Mineral. **104**, 718 (2019).
[80]G. Shen, L. Wang, R. Ferry, H.-K. Mao, and R. J. Hemley, J. Phys.: Conf. Ser. **215**, 012191 (2010).
[81]D. A. Dickey and W. A. Fuller, Econometrica **49**, 1057 (1981).
[82]J. G. MacKinnon, "Critical values for cointegration tests," Working Paper No. 1227, Economics Department, Queen's University, 2010.
[83]S. S. Shapiro and M. B. Wilk, Biometrika **52**, 591 (1965).
[84]A. J. Campbell, C. T. Seagle, D. L. Heinz, G. Shen, and V. B. Prakapenka, Phys. Earth Planet. Inter. **162**, 119 (2007).
[85]C. E. Yen, Q. Williams, and M. Kunz, J. Geophys. Res.: Solid Earth **125**, e2020JB020006, https://doi.org/10.1029/2020jb020006 (2020).
[86]A. Kubo, T. Suzuki, and M. Akaogi, Phys. Chem. Miner. **24**, 488 (1997).
[87]A. R. Thomson, M. J. Walter, S. C. Kohn, and R. A. Brooker, Nature **529**, 76 (2016).
[88]J. Braithwaite and L. Stixrude, Geophys. Res. Lett. **46**, 2037, https://doi.org/10.1029/2018gl081805 (2019).
[89]S. Klotz, J.-C. Chervin, P. Munsch, and G. Le Marchand, J. Phys. D: Appl. Phys. **42**, 075413 (2009).
[90]A. K. Singh and T. Kenichi, J. Appl. Phys. **90**, 3269 (2001).
[91]K. Takemura and A. Dewaele, Phys. Rev. B **78**, 104119 (2008).
[92]S. M. Dorfman, V. B. Prakapenka, Y. Meng, and T. S. Duffy, J. Geophys. Res.: Solid Earth **117**, B08210, https://doi.org/10.1029/2012jb009292 (2012).
[93]E. Menéndez-Proupin and A. K. Singh, Phys. Rev. B **76**, 054117 (2007).
[94]Z.-Y. Zeng, C.-E. Hu, L.-C. Cai, X.-R. Chen, and F.-Q. Jing, J. Phys. Chem. B **114**, 298 (2010).
[95]S. M. Dorfman, F. Jiang, Z. Mao, A. Kubo, Y. Meng, V. B. Prakapenka, and T. S. Duffy, Phys. Rev. B **81**, 174121 (2010).
[96]R. R. Gattass and E. Mazur, Nat. Photonics **2**, 219 (2008).
[97]M. J. Pfeifenberger, M. Mangang, S. Wurster, J. Reiser, A. Hohenwarter, W. Pfleging, D. Kiener, and R. Pippan, Mater. Des. **121**, 109 (2017).
[98]A. D. Smith, J. Donoghue, A. Garner, B. Winiarski, E. Bousser, J. Carr, J. Behnsen, T. L. Burnett, R. Wheeler, K. Wilford, P. J. Withers, and M. Preuss, Exp. Mech. **59**, 1113 (2019).
[99]E. F. O'Bannon III, Z. Jenei, H. Cynn, M. J. Lipp, and J. R. Jeffries, Rev. Sci. Instrum. **89**, 111501 (2018).
[100]G. Pacchioni, Nat. Rev. Phys. **1**, 100 (2019).
[101]R. Khubbutdinov, A. P. Menushenkov, and I. A. Vartanyants, J. Synchrotron Radiat. **26**, 1851 (2019).
[102]C. Herzberg, K. Condie, and J. Korenaga, Earth Planet. Sci. Lett. **292**, 79 (2010).